

Highly Accurate DSM Reconstruction Using Ku-Band Airborne InSAR

Yu Okada, Chie Hirao, Takeshi Horiuchi, Yoshihisa Hara, Jonathan Yedidia, Ali Azarbayejani,
Noboru Oishi, Masatada Furuhashi, Nobuo Kumagai, Shouji Morioka, Yoshihiko Kato

TR2007-064 August 2007

Abstract

We present a newly developed airborne InSAR system incorporating a novel phase unwrapping algorithm, capable of retrieving a highly accurate Digital Surface Model (DSM). The SAR sensor system, with a spatial resolution of 30 cm, is carried on an airborne platform which has two antennas placed at a baseline length of 1 meter. We have established a DSM reconstruction processing technique, which includes the new "Iterated Conditional Modes-Minimum Cost Flow" (ICM-MCF) phase-unwrapping algorithm. The ICM-MCF algorithm finds a locally optimal configuration of unwrapped phases under a well-characterized statistical model of the terrain and noise. An experimental field observation was carried out in Tsukuba, Japan. The DSM was generated, and the height accuracy of the SAR-DSM was evaluated by comparing with laser profiler data. For 50 cm X 50 cm mesh an accuracy of better than 50 cm in height was confirmed.

IGARSS 2007

This work may not be copied or reproduced in whole or in part for any commercial purpose. Permission to copy in whole or in part without payment of fee is granted for nonprofit educational and research purposes provided that all such whole or partial copies include the following: a notice that such copying is by permission of Mitsubishi Electric Research Laboratories, Inc.; an acknowledgment of the authors and individual contributions to the work; and all applicable portions of the copyright notice. Copying, reproduction, or republishing for any other purpose shall require a license with payment of fee to Mitsubishi Electric Research Laboratories, Inc. All rights reserved.

Highly accurate DSM reconstruction using Ku-band airborne InSAR

Yu Okada, Chie Hirao, Takeshi Horiuchi, Yoshihisa Hara,
Jonathan S. Yedidia, Ali Azarbajegani, Noboru Oishi, Masatada Furuhashi,
Nobuo Kumagai, Shouji Morioka, Yoshihiko Kato

TR-2007-064 July 2007

Abstract

We present a newly developed airborne InSAR system incorporating a novel phase unwrapping algorithm, capable of retrieving a highly accurate Digital Surface Model (DSM). The SAR sensor system, with a spatial resolution of 30 cm, is carried on an airborne platform which has two antennas placed at a baseline length of 1 meter. We have established a DSM reconstruction processing technique, which includes the new “Iterated Conditional Modes–Minimum Cost Flow” (ICM-MCF) phase-unwrapping algorithm. The ICM-MCF algorithm finds a locally optimal configuration of unwrapped phases under a well-characterized statistical model of the terrain and noise. An experimental field observation was carried out in Tsukuba, Japan. The DSM was generated, and the height accuracy of the SAR-DSM was evaluated by comparing with laser profiler data. For 50 cm x 50 cm mesh an accuracy of better than 50 cm in height was confirmed.

This work may not be copied or reproduced in whole or in part for any commercial purpose. Permission to copy in whole or in part without payment of fee is granted for nonprofit educational and research purposes provided that all such whole or partial copies include the following: a notice that such copying is by permission of Mitsubishi Electric Research Laboratories, Inc.; an acknowledgment of the authors and individual contributions to the work; and all applicable portions of the copyright notice. Copying, reproduction, or republishing for any other purpose shall require a license with payment of fee to Mitsubishi Electric Research Laboratories, Inc. All rights reserved.

Published in the Proceedings of the 2007 IEEE International Geoscience and Remote Sensing Symposium (IGARSS 2007).

Highly accurate DSM reconstruction using Ku-band airborne InSAR

Yu Okada^{†◊}, Chie Hirao[†], Takeshi Horiuchi[†], Yoshihisa Hara[†]

Jonathan S. Yedidia[‡], Ali Azarbayejani[‡],

Noboru Oishi^{*}

Masatada Furuhata^{*}, Nobuo Kumagai^{*}, Shouji Morioka^{*}, Yoshihiko Kato^{*}

[†]:Kamakura Works, Mitsubishi Electric Corporation, 325 Kamimachiya, Kamakura, Kannagawa, 247-8520, Japan

[‡]:Mitsubishi Electric Research Labs, Cambridge, MA 02139 USA

^{*}:Information Technology R&D Center, Mitsubishi Electric Corporation, 5-1-1 Ofuna, Kamakura, Kanagawa, 247-8501, Japan

^{*}:JAROS, 2-24-2 Hatchobori, Chuo-ku, Tokyo, 104-0032, Japan

[◊]:Okada.Yu@eb.MitsubishiElectric.co.jp

Abstract— We present a newly developed airborne InSAR system incorporating a novel phase unwrapping algorithm, capable of retrieving a highly accurate Digital Surface Model (DSM). The SAR sensor system, with a spatial resolution of 30 cm, is carried on an airborne platform which has 2 antennas placed in a baseline length of 1 m. We have established a DSM reconstruction processing technique, which includes the new “Iterated Conditional Modes-Minimum Cost Flow” (ICM-MCF) phase-unwrapping algorithm. The ICM-MCF algorithm finds a locally optimal configuration of unwrapped phases under a well-characterized statistical model of the terrain and noise. An experimental field observation was carried out in Tsukuba, Japan. The DSM was generated, and the height accuracy of the SAR-DSM was evaluated by comparing with laser profiler data. For 50 cm × 50 cm mesh, an accuracy of better than 50 cm in height was confirmed.

I. INTRODUCTION

For prompt monitoring and response to natural disasters, such as earthquake, landslide, and flood, high resolution 3-dimensional and all-weather remote sensing instruments are essential. So far, 3-dimensional data has been generated by using optical instruments, such as laser profilers and CCD-cameras. However, such instruments have difficulty in cloudy weather, or at night, and can only be used in a very narrow swath area. SAR interferometry, which is available in all weather conditions and over a broad swath area, is a promising approach for future 3-dimensional mapping systems.

We have therefore newly developed a new Ku-band airborne InSAR system and DSM reconstruction algorithm with the goal of retrieving a highly accurate DSM. Section II presents our Ku-band InSAR system. In Section III, an overview of the data processing method for DSM reconstruction is presented, and a novel phase unwrapping algorithm is described. Finally, Section IV presents field test results and evaluation summaries of the height accuracy for the DSM.

II. KU-BAND AIRBORNE SAR SYSTEM

In order to obtain a 3-dimensional map with high accuracy, SAR sensors need a good spatial resolution. The Ku-band, with its broad available bandwidth, was therefore selected. Table I shows the system parameters of our Ku-band InSAR system.



Fig. 1. Ku-band airborne InSAR system.

We used a central frequency of 16.7 GHz, and a bandwidth of 500 MHz. A spatial resolution of 30 cm in both the azimuth and range direction can be obtained. Dual antennas were installed perpendicular to the along-track direction, as shown in Figure 1. The baseline length is set at 1 m, and a Traveling Wave Tube (TWT) with a power of 300 W was utilized as the transmitter. The pulse is transmitted from the master antenna, and the reflected pulse is received by the master and slave antenna alternately, following the pulse repetition interval. Since two SAR images are available simultaneously in an observation, the SAR-DSM can be obtained from a single pass.

TABLE I
PARAMETERS OF THE KU-BAND AIRBORNE SAR

Item	Parameters
Center frequency	16.7 GHz
Bandwidth	500 MHz
Transmitted Power	300 W
Antenna Baseline length	1 m
Off-nadir angle	50 °
Range resolution	30 cm
Azimuth resolution	30 cm

III. INSAR DATA PROCESSING

A. Data processing flow

The data processing, as shown in Figure 2, begins from a pair of SAR complex images. The two images are first

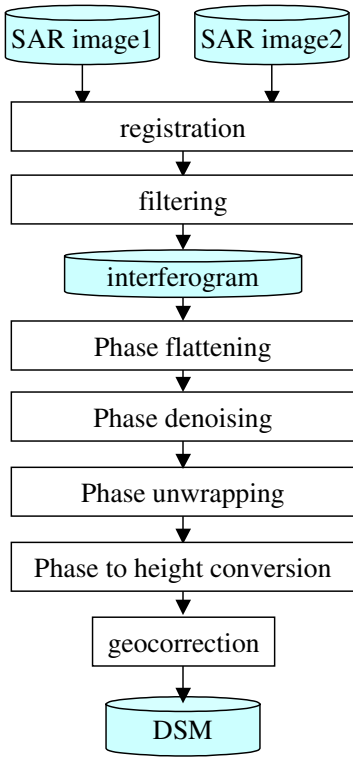


Fig. 2. InSAR data processing flow for DSM reconstruction.

precisely registered. Then the registered images are filtered to improve the signal to noise ratio, and an interferogram is generated. After a phase flattening step and a denoising step, the interferogram is unwrapped. A height is calculated from the unwrapped data, and the final DSM can then be obtained from the geocorrection using reference ground control points (GCPs).

In the next section, we describe in detail our new phase-unwrapping algorithm, which is a key step in the processing flow for obtaining a highly accurate DSM.

B. ICM-MCF phase-unwrapping algorithm

The ICM-MCF algorithm finds a locally optimal configuration of unwrapped phases under a well-characterized statistical model of the terrain and noise that is defined using the “factor graph” formalism [1]. The algorithm iterates between an ICM algorithm that optimizes re-wrapped phases and an MCF algorithm that optimizes integer shifts.

1) The factor graph for the phase-unwrapping problem:

The ICM-MCF algorithm is a probabilistic approach, which aims to find a configuration of re-wrapped phases and integral phase-shifts that is most probable given the input interferogram of noisy wrapped phases (and possibly a coherence map). To quantify the probability of a set of output re-wrapped phases and integer shifts, we define an explicit statistical model using a factor graph, which is at the same time a very convenient graphical device for visualizing the data structures that are used in the algorithm.

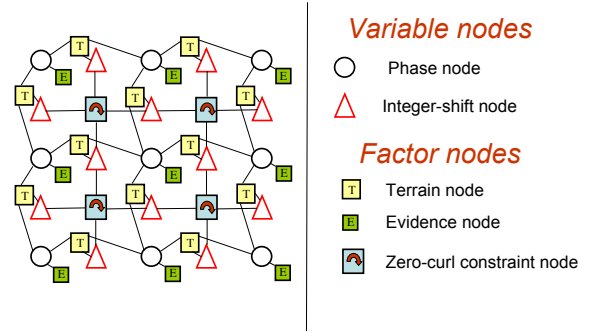


Fig. 3. The factor graph that we use to define the probabilities (or equivalently costs) of a given configuration of re-wrapped real phases and integer shifts. The total cost of a configuration of variable nodes is the sum of the costs for all the factor nodes, given the configuration of the variable nodes.

Factor graphs are bi-partite graphs containing “variable” nodes and “factor” nodes [1]. In our factor graph (see Figure 3), there are two types of variable nodes: “re-wrapped phase” nodes (hereafter simply called “phase” nodes) and “integer-shift” nodes. The phase variable nodes are measured in units of cycles of 2π radians, and take on values in the range $[0.0, 1.0]$. The integer-shift variable nodes take integral values; for relatively smooth terrain, we use the three values $\{-1, 0, +1\}$. The phase nodes and integer shift nodes together implicitly characterize the desired unwrapped phase surface: the phase nodes give the fractional part, while the integer shifts can be used to recover the integral part of the unwrapped phase surface.

The factor graph also uses three types of factor nodes: “evidence” nodes, “terrain” nodes, and “zero-curl constraint” nodes (hereafter called “curl” nodes). Each factor node assigns a “cost” to the configurations of the variable nodes to which it is connected. We find the maximum probability configuration by minimizing the overall cost obtained by summing the costs associated with each factor node.

Each curl node is connected to four integer-shift nodes. The curl nodes enforce the constraint that in a properly defined surface, as one travels around any short loop of four adjacent phase positions (referred to hereafter as “pixels,”), returning to the same phase position, one must return to the same unwrapped phase. To enforce this constraint, a cost of infinity is assigned to any “illegal” configuration of integer-shifts that do not sum to zero when going around a loop, while a cost of zero is assigned to the legal configurations that do sum to zero.

Each terrain node is connected to two adjacent phase nodes and one integer-shift node. The terrain nodes model the fact that the unwrapped phases of two adjacent pixels are more likely to be close to each other than they are to be far from each other. For example, if a pixel has a wrapped phase of $.95$, and an adjacent pixel has a wrapped phase value of $.05$,

then we would expect that there is probably an integer shift of +1 connecting them. We use a terrain node cost linear in the difference between the unwrapped phases, which translates to a Laplacian probability distribution for the unwrapped phases, which is realistic for most terrain.

For the evidence nodes, we can use a variety of different functions, representing shot or Gaussian noise and incorporating reliability information. We assumed a linear relationship between the coherence of a pixel and a cost $C_{Evidence}$ for that pixel, except that $C_{Evidence}$ was zero for “unreliable” pixels that had a coherence below a minimum threshold.

Intuitively, these cost functions cause the algorithm to try to closely match the re-wrapped phase value to the received phase if the coherence is high; while if the coherence is low, the algorithm prefers to maintain smooth terrain and will assume that any spikes in the phase values given by the interferogram are probably due to noise.

2) *The Optimization Algorithm:* Given our factor graph, one can use a variety of optimization algorithms to try to find the most probable configuration. Since the optimization of the factor graph is an NP-hard problem, any efficient algorithm can only hope to find approximate solutions. Our ICM-MCF algorithm is highly efficient in both memory and time—it is linear with the number of pixels, with small prefactors that allow for practical implementation. The ICM-MCF algorithm provably finds a locally optimal configuration of the integer-shifts and phases.

In each iteration of the over-all ICM-MCF algorithm we first optimize the integer shifts, while holding the phases fixed, by running the minimum-cost-flow (MCF) algorithm [2]. Then half of the phases are optimized while holding their neighboring phases and the integral shifts fixed (an ICM step). The MCF algorithm is then re-run, followed by an optimization of the other half of the phases. Only a small number of iterations (less than 15) will typically be required for convergence, even for images containing more than four million phase nodes.

The MCF algorithm assumes that the latest computed phases are correct, and tries to find the integer-shifts that will be least costly in terms of the terrain costs. The problem is transformed into a flow problem on a dual network defined by the curl nodes, connected to each other by the integer-shift nodes.

The ICM algorithm (see Figure 4) arranges the phases into a checkerboard pattern, and will output new optimized phase values for half of the phases (e.g. the “black” ones), assuming the other half (the “white” ones) and all of the integer-shift values are fixed. The optimization for a particular target phase is local, affected only by the local evidence node and the cost from the four neighboring terrain nodes. For each neighboring terrain node, we compute a phase value (called the “advice”) which is the optimal value of the target phase given just that terrain node. Because of the linear dependence in the terrain cost on the value of the phase, it is possible to prove that the optimal local phase given the four neighboring terrain nodes is the median value of the advice. This optimal value is then compared with the cost of agreeing or disagreeing with the

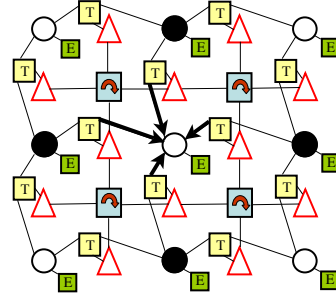


Fig. 4. During an ICM phase of the algorithm, the phase nodes are divided into a checkerboard pattern. In one of those phases, each “white” phase node is optimized, and receives “advice” about its correct value from its four neighboring “black” phase nodes, which are held fixed along with the integer-shift nodes. In the next ICM phase, the white nodes are held fixed and the black nodes are optimized.

local evidence node, and the overall lowest cost phase for each target node is computed.

The ICM-MCF algorithm can easily account for different reliability in the values of received phases (as obtained, for example, from a coherence map) by adjusting the noise model. This contrasts favorably with previous approaches that used factor graphs but without an adjustable noise model [3]. The algorithm is similar in flavor to the $Z\pi M$ algorithm introduced by Dias and Leitao [4], but the statistical models are different, including the important difference that the ICM-MCF algorithm rigorously enforces the zero-curl constraint at each iteration.

IV. FIELD TEST RESULTS

A. SAR images and DSM

A field experiment was conducted in the Tsukuba area in Japan, where there is an agricultural field connecting to the foot of a mountain. This area was selected because reference DSM data measured by the laser profiler was available. The experiment was conducted in October 2006. For the geocorrection described in Section III, 8 corner reflectors are set during the experiment as GCPs.

Figure 5(a) shows the SAR amplitude image of the master antenna after the geocorrection. Agricultural field, woods, and ditches are clearly visible. From the signal processing flow described in Section III, the SAR DSM was generated. Figure 5(b) shows the SAR DSM in the same area as Figure 5(a). The mesh size of the DSM is set at $50\text{ cm} \times 50\text{ cm}$. The altitude rises as it approaches the mountain from the agricultural field, and it is consistent with the topography in this field. A zoomed image of the DSM in the agricultural field is shown in Figure 5(c), and photographs taken by a ground investigation in the agricultural field steps are shown in Figure 5(d). The step-structure in the agricultural field can be clearly seen in the zoomed DSM image.

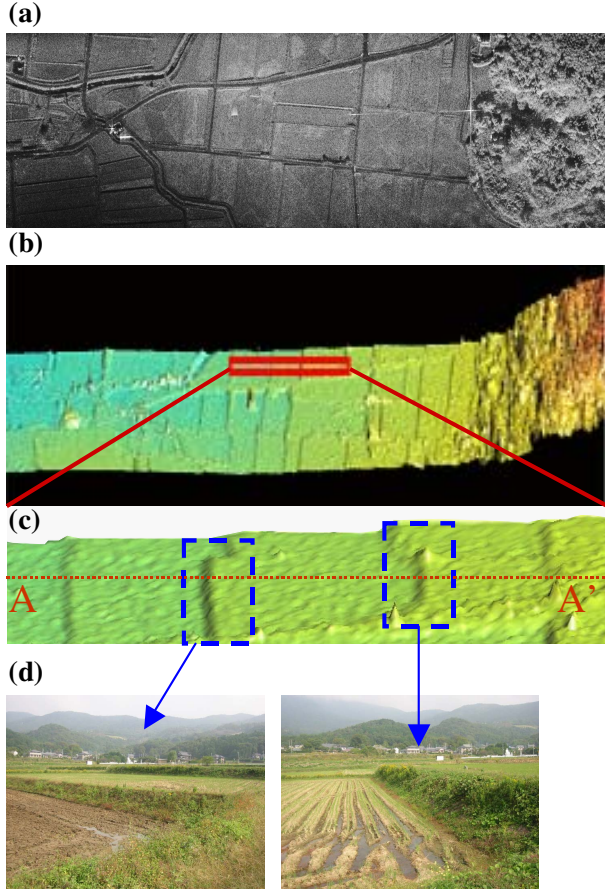


Fig. 5. Field test results:(a)SAR amplitude (b) SAR DSM (c) SAR DSM(zoomed) (d)Ground truth

B. DSM Height Accuracy

Here we compare the reconstructed SAR DSM data with the reference laser data. Figure 6 shows a one-dimensional sliced height profile of the SAR DSM in the agricultural filed steps (see Figure 5(c)), compared with the reference laser profiler data. Although spikes remain in the SAR DSM, the overall structure of the agricultural field steps is consistent with the laser data, which means that the SAR DSM reconstruction works correctly.

To assess the height retrieval accuracy quantitatively, we define an offset error, ΔH and a standard deviation of the SAR DSM, σ_H , with respect to the laser data, as

$$\Delta H = \frac{1}{N} \sum_{i=1}^N |H_{\text{SAR}}(X_i) - H_{\text{laser}}(X_i)| \quad (1)$$

$$\sigma_H = \sqrt{\frac{1}{N} \sum_{i=1}^N (H_{\text{SAR}}(X_i) - H_{\text{laser}}(X_i))^2}, \quad (2)$$

where N is a number of data points, and $H_{\text{SAR}}(X_i)$ and $H_{\text{laser}}(X_i)$ are a height in position X_i derived from the SAR and laser, respectively. Evaluation results in terms of the standard deviation and the offset error are summarized in

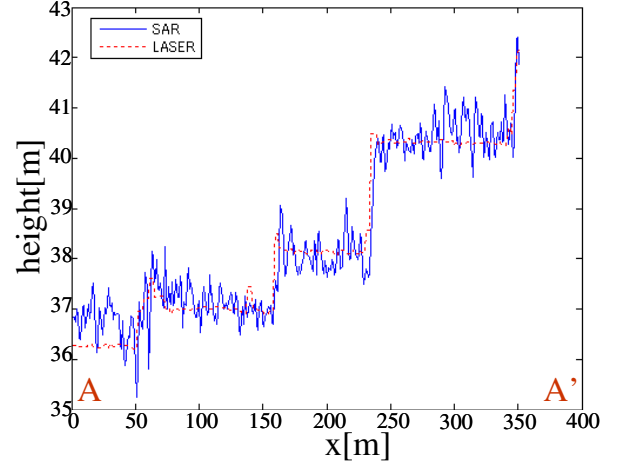


Fig. 6. Height accuracy in the sliced region.

Table II. We have obtained an accuracy of less than 50 cm error in 50 cm \times 50 cm mesh data.

TABLE II
EVALUATION RESULT OF THE SAR DSM.

Item	Value
Mesh size	50 cm \times 50 cm
Height error (offset) ΔH	37 cm
Height error (standard deviation) σ_H	47 cm

V. CONCLUSIONS

We have developed a Ku-band InSAR system, and attempted to generate highly accurate DSM by SAR interferometry. We proposed a novel phase unwrapping algorithm and applied it to the Ku-band field data. As a result, a height accuracy of less than 50 cm error for a 50 cm \times 50 cm mesh can be achieved. Since our InSAR system has two antennas and can be considered single pass interferometry, Ku-InSAR system has great promise to become a future 3-dimensional accurate data infrastructural establishment.

ACKNOWLEDGMENT

We gratefully acknowledge the help of the Mechanical Social Systems Foundation(MSSF) in providing the data used in this study.

REFERENCES

- [1] F. R. Kschischang, B. J. Frey, and H. Loeliger. Factor graphs and the sum-product algorithm. *IEEE Trans. Inform. Theory*, 47:498–519, February 2001.
- [2] M. Costantini. A novel phase unwrapping method based on network programming. *IEEE Transactions on Geoscience and Remote Sensing*, 36:813–821, May 1998.
- [3] B. J. Frey, R. Koetter, and N. Petrovic. Very loopy belief propagation for unwrapping phase images. In *Advances in Neural Information Processing Systems 14*. 2001.
- [4] J. M. B Dias and J. M. N. Leitao. The Z π M algorithm: a method for interferometric image reconstruction in SAR/ SAS. *IEEE Trans. Image Processing*, 11:408–422, 2002.